Magnetic Reconnection in Toroidal η_i Mode Turbulence

A. Zeiler
Max-Planck-Institut für Plasmaphysik, EURATOM Association, 85748 Garching, Germany

J. F. Drake and B. N. Rogers
Institute for Plasma Research, University of Maryland, College Park, Maryland 20742
(Received 7 June 1999)

Based on three-dimensional simulations of the Braginskii equations we show that for typical plasma-edge parameters the saturation of electromagnetic toroidal η_i mode turbulence is controlled by the self-generation and subsequent annihilation of radial magnetic field perturbations. This should be contrasted with the electrostatic limit, where the growth of the linear η_i mode is terminated by the onset of sheared flow modes driven by the radial plasma streams. The impact of the saturation amplitude on the transport level is substantial and is not in accord with simple mixing length arguments, suggesting that electromagnetic effects should generally be included in simulations of η_i mode turbulence.

PACS numbers: 52.35.Ra, 52.35.Kt, 52.55.Fa

The overall performance of magnetic confinement experiments such as tokamaks and stellarators crucially depends on the anomalous transport, which is generally believed to originate from plasma turbulence. Whereas in the cool outer parts of the plasma edge the turbulence seems to be mainly driven by resistive instabilities [1], toroidal η_i mode turbulence plays a dominant role in the hotter parts of the plasma edge and in the plasma core [2,3]. In both regimes numerical simulations were typically carried out in the electrostatic limit. Recent electromagnetic simulations, however, demonstrate that magnetic fluctuations play a crucial role at the edge, where resistive instabilities dominate [4–6], and emphasize the need for fully electromagnetic investigations in the adjacent η_i mode regime. In this Letter we show that magnetic fluctuations strongly affect η_i mode turbulence in the hotter parts of the plasma edge in a manner unexpected from linear theory. Linearly electromagnetic effects shift the toroidal η_i mode to longer wavelength. Thus, one would expect an increase of the transport level. Our nonlinear simulations, however, exhibit a strong drop of the transport rates. The reason for this surprising behavior is linked to the mechanism which saturates the η_i mode turbulence. Instabilities driven by unfavorable curvature which have a strong ballooning character form radial streams, and it is the breakup of these streams by secondary instabilities which controls the saturation of the instability and ultimately the level of transport [4,7]. In the electrostatic limit of the η_i instability the dominant secondary instability is the sheared flow mode, which has a finite radial wave vector and therefore shears apart the radial streams associated with the linear instability [1,2]. In the electromagnetic regime the radial streams drag the toroidal magnetic field, producing radial magnetic perturbations which alternate sign as a function of the poloidal angle. The magnetic reconnection of these radial magnetic field perturbations produces regions of locally intense flows which break apart the radial streams, supplanting the shear flow modes as the dominant saturation mechanism of the η_i instability. Consequently, electrostatic and electromagnetic turbulence follows a fundamentally different dynamics, and a comparison between the two merely based on the linear properties of the η_i mode necessarily fails.

Our investigations are based on the drift-Braginskii equations with isothermal electrons [6,8], which are solved in a three-dimensional flux-tube domain [9],

$$(2\pi)^2\alpha_m(\partial_t\psi + \alpha_d\partial_y\psi) - \nabla_\parallel(\phi - \alpha_d n) = J\,, \quad (1)$$

$$\nabla_\perp \cdot d_t\nabla_\perp(\phi + \tau\alpha_d p_i) + \hat{C}(p + G) - \nabla_\parallel J = 0\,, \quad (2)$$

$$d_t n + \partial_y\phi - [\epsilon_n\hat{C}(\phi - \alpha_d n) - \epsilon_v\nabla_\parallel v_\parallel + \alpha_d\epsilon_n(1+\tau)\nabla_\parallel J] = 0\,, \quad (3)$$

$$d_t T_i + \eta_i\partial_y\phi - \frac{2}{3}\left[\epsilon_n\hat{C}\left(\phi - \alpha_d n + \frac{5}{2}\tau\alpha_d T_i\right) - \epsilon_v\nabla_\parallel v_\parallel + \alpha_d\epsilon_n(1+\tau)\nabla_\parallel J\right] - \frac{2}{3}\kappa_i\nabla_\parallel[\nabla_\parallel T_i + (2\pi)^2\alpha_m\eta_i\partial_y\psi] = 0\,, \quad (4)$$

$$d_t v_\parallel = -\epsilon_v[\nabla_\parallel(p + 4G) + (2\pi)^2\alpha\,\partial_y\psi]\,, \quad (5)$$

with $J = \nabla_\perp^2\psi$, $p = n + \tau T_i/(1+\tau)$, $p_i = n + T_i$, $G = 2\gamma_p[\hat{C}(\phi + \tau\alpha_d p_i) - 4(\epsilon_v/\epsilon_n)\nabla_\parallel v_\parallel]$, and the operators $\nabla_\perp^2 = [\partial_x + \Lambda(z)\partial_y]^2 + \partial_y^2$, $\nabla_\parallel = \partial_z + (2\pi)^2\alpha_m\mathbf{z}\times\nabla\psi\cdot\nabla$, $d_t = \partial_t + \mathbf{z}\times\nabla\phi\cdot\nabla$, $\hat{C} = [\cos(2\pi z) + \Lambda(z)\sin(2\pi z) - \epsilon]\partial_y + \sin(2\pi z)\partial_x$ with the shear function $\Lambda(z) = 2\pi\hat{s}z - \alpha\sin(2\pi z)$ and $\epsilon = a/R$. To facilitate the comparison with previous work [1,4,6], we use the normalization for resistive

ballooning turbulence [9] $t_0 = (RL_n/2)^{1/2}/c_s$, $L_\parallel = 2\pi qR$, and $L_\perp = L_\parallel/(1.96\omega_{ce}\tau_e\omega_{ci}t_0)^{1/2}$. This yields the diamagnetic parameter $\alpha_d = v_* t_0/L_\perp$ with v_* the electron diamagnetic velocity, $\epsilon_n = 2L_n/R$, $\epsilon_v = \epsilon_n^{1/2}/(4\pi q)$, $\eta_i = L_n/L_{T_i}$, the ion to electron temperature ratio τ, the parallel heat conductivity κ_i, and the magnetic pumping parameter γ_p. The parameter $\alpha_m = q^2 R\beta/L_n$, finally, is directly related to the usual MHD parameter α by $\alpha = \alpha_m[1 + \eta_i\tau/(1 + \tau)]$.

We start our investigations with a brief discussion of the linear properties of our model at parameters typical for the η_i mode regime. To illustrate the basic mechanisms we drop the parallel heat conduction $\kappa_i = 0$, magnetic pumping $\gamma_p = 0$, the parallel sound wave $\epsilon_v = 0$, magnetic shear $\Lambda(z) = 0$, and the resistivity [right hand side of Eq. (1)], and evaluate the curvature operator at the outside of the torus $\hat{C} = \partial_y$. With the ansatz $\psi, \phi, n, T_i \propto \exp\{i(k_y y + k_z z - \omega t)\}$, we obtain from Eqs. (1) and (3) the relation

$$\left[1 - \frac{1}{\hat{c}_A^2 k_z^2}\frac{\hat{\omega}_*^2}{k_y^2\hat{\rho}_s^2}\left(\frac{\omega}{\hat{\omega}_*} - 1\right)(1 - \epsilon_n)\right]\phi = \left[1 - \frac{1}{\hat{c}_A^2 k_z^2}\frac{\hat{\omega}_*^2}{k_y^2\hat{\rho}_s^2}\left(\frac{\omega}{\hat{\omega}_*} - 1\right)\left(\frac{\omega}{\hat{\omega}_*} - \epsilon_n\right)\right]\alpha_d n\,, \tag{6}$$

with the normalized diamagnetic frequency $\hat{\omega}_* = \alpha_d k_y$, $\hat{\rho}_s^2 \equiv \rho_s^2/L_\perp^2 = \alpha_d^2\epsilon_n(1 + \tau)$, and the normalized Alfvén velocity $\hat{c}_A^2 = 1/[(2\pi)^2\alpha_m]$. Equation (6) shows that the usual adiabatic electron relation $\phi = \alpha_d n$ results only in the electrostatic limit $\hat{c}_A \longrightarrow \infty$, whereas in the general case nonadiabatic effects are important unless $\alpha_m(2\pi/k_z)^2 \ll \epsilon_n$. Hence the importance of electromagnetic effects crucially depends on the parallel wavelength, and we must include the complete parallel dynamics. Therefore we use our three-dimensional initial value code to deduce the linear properties of Eqs. (1)–(5). At moderate gradients $\epsilon_n \gtrsim 0.2$ we recover the well-known electromagnetic stabilization of the toroidal η_i mode [10,11] (Fig. 1a). At steep gradients $\epsilon_n \lesssim 0.2$, which are typical of the plasma edge, however, the mode is destabilized at long wavelength (Fig. 1b). In Figs. 1c and 1d we show the modulus of the perturbation. Whereas in the electrostatic limit (Fig. 1d) ϕ and n are of similar magnitude, n is much larger than ϕ in the electromagnetic case (Fig. 1c), indicating that the electron response is far from adiabatic as expected from Eq. (6). Finally we note that in the electromagnetic calculation ϕ, n, and T_i are peaked at the unfavorable curvature location at the outside of the torus ($z = 0$), whereas the magnetic perturbation ψ vanishes at this place and reaches its maximum at $z = \pm 0.2$.

Following the widely accepted estimate $D \propto \gamma/k_\perp^2$ the linear theory leads to the important prediction that the transport rates should go up significantly if electromagnetic effects are taken into account at the plasma edge. To test this idea we proceed with three-dimensional nonlinear simulations of the complete model Eqs. (1)–(5) using numerical methods described elsewhere [9]. Our runs are carried out at various parameters summarized in Fig. 2 in a box of dimensions $76.4L_\perp \times 80L_\perp \times 3L_\parallel$, which

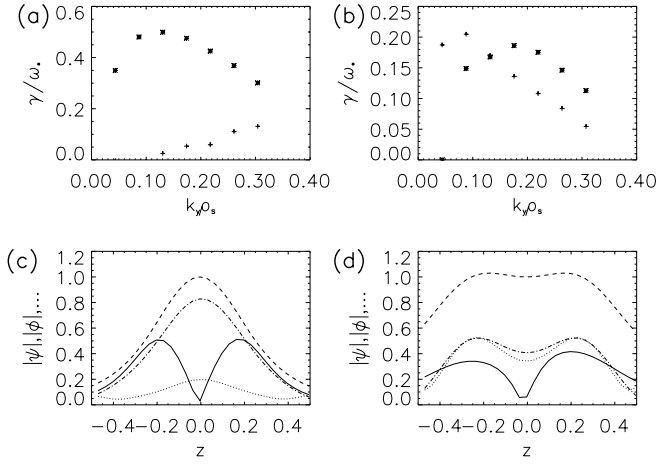

FIG. 1. Linear growth rate of the toroidal η_i mode. (a),(b): Full numerical solution for $\tau = 1$, $\eta_i = 2.5$, $\alpha_d = 1.25$, $\kappa_i = 0.005$, $\gamma_p = 0.075$, $\hat{s} = 1$, $\epsilon = 0.2$, $\epsilon_v = 0.008$, $\alpha = 0$ (stars), $\alpha = 0.675$ (crosses), $\epsilon_n = 0.3$ (a), $\epsilon_n = 0.1$ (b). (c),(d): Shape along z of the linear solutions displayed in (b) at $k_y\rho_s = 0.175$; $|\psi|$ (solid), $|\phi|$ (dotted), $|T_i/2|$ (dashed), $|n|$ (dash-dotted); $\alpha_m = 0.675$ (c), $\alpha_m = 0$ (d).

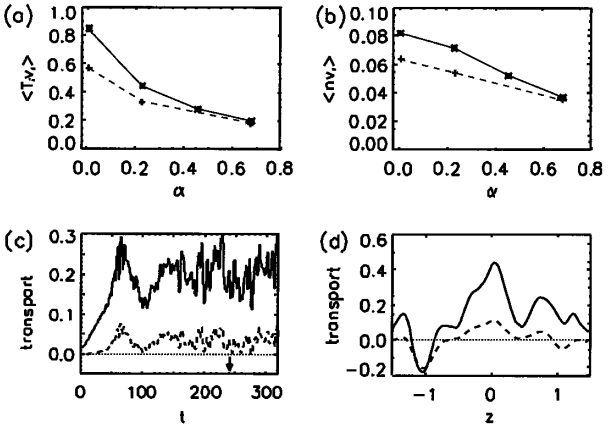

FIG. 2. Transport rates in nonlinear simulations. The simulations have been carried out with $\alpha_d = 1.25$, $\eta_i = 2.5$, $\tau = 1$, $\hat{s} = 1$, $\epsilon = 0.2$. κ_i and γ_p are chosen according to $\kappa_i = 0.01\tau^{5/2}\alpha_d^2\epsilon_n(1 + \tau)$, and $\gamma_p = 0.16\pi^2 q^2\kappa_i$. (a),(b): Ion heat flux $\langle T_i v_r\rangle$ (a), particle flux $\langle n v_r\rangle$ (b) versus α, for $\epsilon_n = 0.07$ (crosses, dashed line) and $\epsilon_n = 0.1$ (stars, solid line). (c) Heat flux (solid) and particle flux (dashed) versus time in the simulation with $\alpha = 0.675$ and $\epsilon_n = 0.07$. (d) Variation of heat flux (solid) and particle flux (dashed) along the magnetic field at $t = 244.5$ [marked by a small arrow in (c)]. The outside of the torus corresponds to $z = 0, \pm 1$.

is resolved by $192 \times 192 \times 90$ collocation points. Most surprisingly our results are in strong contradiction to the linear predictions: The turbulent transport rates drop by about a factor of 3 as we proceed from the electrostatic limit ($\alpha = 0$) into the electromagnetic regime (Figs. 2a and 2b). At large α the fluxes exhibit large fluctuations (Fig. 2c) and may even become negative corresponding to inward transport (Fig. 2d). As a characteristic feature of the electromagnetic turbulence we observe highly localized eddies in the magnetic field as well as in the $\mathbf{E} \times \mathbf{B}$ velocity. The velocity within these eddies considerably exceeds average levels, indicating that the vortices are driven by a source different from the usual inverse cascade of kinetic energy. These strong flows cause the fluctuations of the fluxes, and can result in localized spikes of the transport rates with either sign.

The failure of the linear estimate to predict the change of the transport rates due to electromagnetic effects shows that magnetic fluctuations must also strongly affect the nonlinear saturation of the fluctuations. The fundamental change of the nonlinear dynamics is underscored by the presence of the fast rotating eddies and the large localized fluxes in the direction opposite to the equilibrium gradients. A more detailed analysis of the time evolution exhibits that these eddies originate from regions where major changes of the magnetic topology occur. Figure 3 shows such an event: In Fig. 3a the magnetic field consists of two oppositely directed bands of magnetic flux, which are separated by a chain of islands. About ten time units later the sheared structure is completely destroyed (Fig. 3b). Right at the location where the change in the magnetic field takes place, we observe a spike of inward transport (Fig. 2d). Thus, magnetic reconnection seems to play a dominant role in the overall dynamics, being responsible for the sudden changes of the transport rates.

To gain more insight into the physical mechanisms that determine the nonlinear dynamics, we now study the saturation of the toroidal η_i mode, where the system makes the transition from the linear growth phase to stationary turbulence. For this purpose we start a simulation with the linear eigenfunction displayed in Fig. 1c as the initial condition. When the toroidal η_i mode grows to finite amplitude, its mode structure becomes unstable to secondary instabilities, which excite modes with $k_x \neq 0$ and destroy the linear pattern. Figure 4 shows the magnetic perturbation ψ at $z = 0.17$ during the saturation process. Initially we observe oppositely directed bands of magnetic field, produced as the flows drag the toroidal magnetic field in the radial direction (see linear eigenfunction in Fig. 4a). A few time units later magnetic islands become visible (Fig. 4b), until at sufficiently large amplitude the magnetic field reconnects (Figs. 4c and 4d). At the same time we observe a spike of inward transport at $z = 0$ and the formation of a localized magnetic eddy, similar to those discussed earlier. Thus the key manifestations of the turbulence already appear at this early stage of the nonlinear dynamics.

Figure 4 suggests the physical mechanism responsible for the breakup of the linear mode structure and the transition to turbulence: in the presence of resistivity (or other effects such as electron inertia that break the frozen in flux constraint), a sheared magnetic field as in Fig. 4a is unstable to the formation of magnetic islands, and reconnection eventually leads to the complete destruction of the banded magnetic field structure. The relevant mode in this case is essentially a periodic version of the double tearing mode [12]. To quantitatively confirm this interpretation we performed two-dimensional simulations of the sheared magnetic configuration as it arises from the toroidal η_i mode at $z \simeq 0.2$. We focus on the nonlinear evolution, since the linear stage is not relevant due to the presence of finite amplitude perturbations in the turbulent state. In agreement with previous work [13,14], the

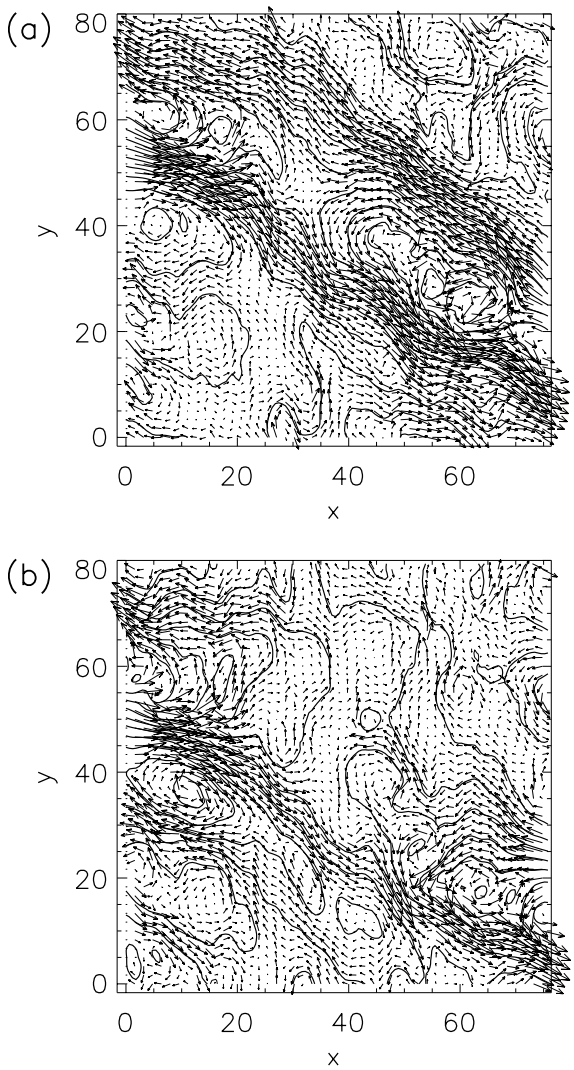

FIG. 3. Magnetic reconnection at a late state of the simulation discussed in Figs. 2c and 2d. The plots show the contours of ψ as well as the resulting magnetic field $\mathbf{B} = \mathbf{z} \times \nabla\psi$, represented by arrows, in the plane $z = -0.83$. (a) Taken at $t = 234$, and (b) at $t = 247$.

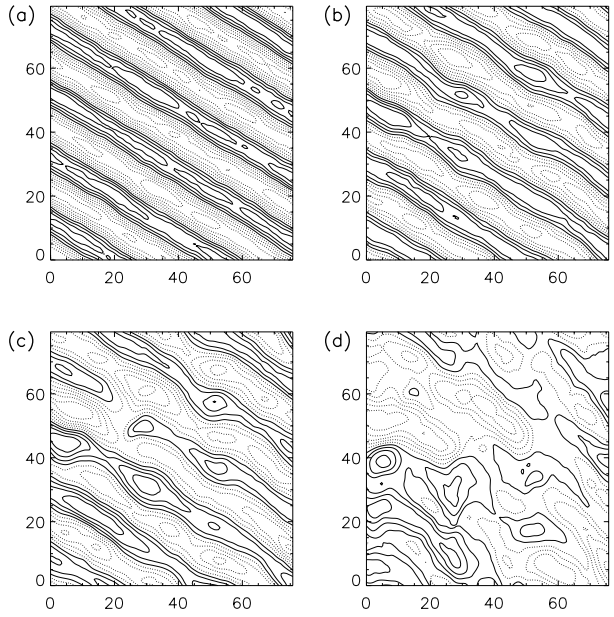

FIG. 4. Structure of the magnetic field during the saturation of the toroidal η_i mode. The plots show contours of the magnetic perturbation ψ in the plane $z = 0.17$, the solid lines corresponding to $\psi > 0$ and the dotted lines to $\psi < 0$. The poloidal angle increases upwards and the equilibrium gradients point to the left. (b) Taken at $t_b = t_a + 8$, (c) at $t_c = t_a + 11.5$, and (d) at $t_d = t_a + 19$.

growth rate of the reconnection mode in this case is insensitive to the resistivity and is given by $\gamma_{\text{reconn}} \simeq 0.2 k_y V_A$, where $V_A = 2\pi\alpha_m^{1/2} k_y \psi$ is based on the typical strength of magnetic field perturbations generated by the toroidal η_i mode. The insensitivity to resistivity is consistent with the results of a further test simulation, in which the transport did not change despite a factor of 5 reduction of the resistivity. To assess the relative roles of reconnection and shear flow instabilities in the saturation process, one can compare γ_{reconn} to the growth rate of the Kelvin-Helmholtz instability, which is excited by the sheared, alternating pattern of $\mathbf{E} \times \mathbf{B}$ flows arising from the toroidal η_i mode. A maximal estimate of the growth rate in this case is given by $\gamma_{\text{KH}} = 0.3 k_y V_E$ [4]. We thus find $\gamma_{\text{reconn}}/\gamma_{\text{KH}} \sim V_A/V_E$, so reconnection is expected to dominate the saturation process if $V_A/V_E > 1$. This ratio can be estimated by combining the vorticity equation (2) (e.g., $\hat{C} p \sim \nabla_\parallel J$) with Eqs. (3) and (4) (e.g., $p \sim p_0' V_E/\gamma$ for ϵ_n, $\epsilon_\nu < 1$). Together these yield $V_A/V_E \sim \sqrt{\alpha}\, L_{\parallel/}/(qR\gamma t_0)$ or, assuming $L_\parallel \sim \pi q R$ and $\gamma \sim \sqrt{\omega_* \omega_c}$ ($\omega_c \sim \epsilon_n \omega_*$ being the curvature drift frequency), one obtains $V_A/V_E \sim \pi\sqrt{\alpha}/(k_y \rho_s)$. The linear spectrum of unstable modes peaks at $k_y \rho_s < 1$ [see Figs. 1a and 1b] and nonlinearly the turbulence spectrum tends to shift even further to long wavelength. Thus, above a low threshold in α magnetic reconnection rather than sheared flow instabilities play the dominant role in breaking up radial streams of the η_i mode and therefore in controlling the transport level. As a final cross-check, we performed a three-dimensional simulation in which the parallel derivative $\nabla_\parallel$ was linearized. With this modification magnetic reconnection is eliminated and the transport rates went up by more than a factor of 2.

In conclusion, we find that the mechanisms responsible for the saturation of electrostatic and electromagnetic η_i turbulence are distinct. Whereas in the electrostatic limit the linear growth phase of the toroidal η_i mode is terminated by the generation of zonal flows (basically a form of Kelvin-Helmholtz instability), in the general electromagnetic case magnetic reconnection of self-generated magnetic perturbations plays the dominant role. As a consequence, the impact of the electromagnetic effects on the linear growth rate of the instability is, by itself, inadequate to estimate the transport level in the electromagnetic regime. Transport levels must be based on complete nonlinear simulations. Specifically, electromagnetic effects play a dominant role in η_i mode turbulence at the steep gradients typical for the plasma edge, especially in the high-confinement mode (H mode), where α is typically of order unity. Although our calculations were focused on conditions relevant to the plasma edge, the results suggest that magnetic fluctuations should generally be included in investigations of η_i mode turbulence.

[1] A. Zeiler, D. Biskamp, J. F. Drake, and B. N. Rogers, Phys. Plasmas **5**, 2654 (1998).
[2] R. E. Waltz, G. D. Kerbel, and J. Milovich, Phys. Plasmas **1**, 2229 (1994).
[3] M. Kotschenreuther, W. Dorland, M. A. Beer, and G. W. Hammett, Phys. Plasmas **2**, 2381 (1995).
[4] B. N. Rogers and J. F. Drake, Phys. Rev. Lett. **79**, 229 (1997).
[5] B. D. Scott, Plasma Phys. Controlled Fusion **39**, 1635 (1997).
[6] B. N. Rogers, J. F. Drake, and A. Zeiler, Phys. Rev. Lett. **81**, 4396 (1998).
[7] S. C. Cowley, R. M. Kulsrud, and R. Sudan, Phys. Fluids B **3**, 2767 (1991).
[8] A. Zeiler, J. F. Drake, and B. N. Rogers, Phys. Plasmas **4**, 2134 (1997).
[9] A. Zeiler, D. Biskamp, J. F. Drake, and P. N. Guzdar, Phys. Plasmas **3**, 2951 (1996).
[10] J. Y. Kim, W. Horton, and J. Q. Dong, Phys. Fluids B **5**, 4030 (1993).
[11] P. B. Snyder, G. W. Hammett, M. A. Beer, and W. Dorland, Bull. Am. Phys. Soc. **44**, 1013 (1999).
[12] P. L. Pritchett, Y. C. Lee, and J. F. Drake, Phys. Fluids **23**, 1368 (1980).
[13] A. Y. Aydemir, Phys. Fluids B **4**, 3469 (1992); R. G. Kleva, J. F. Drake, and F. L. Waelbroeck, Phys. Plasmas **2**, 23 (1995).
[14] M. Shay, J. F. Drake, B. N. Rogers, and R. Denton, Geophys. Res. Lett. **26**, 2163 (1999).